NANO LETTERS

pubs.acs.org/NanoLett Letter

Atom-Response-Theory-Guided Design of Chiral Niobium Halides with both a Large Nonlinear Coefficient and Strong Chiroptical Nonlinearity

Wenting Liu,[†] Xin Zeng,[†] Wenkai Zhao, Haolin Lu, Hebin Wang, Xinyi Niu, Zhaoyu Wang, Tianyin Shao, Sehrish Gull, Bing Sun, Hao-Li Zhang, Xinfeng Liu, Yongsheng Chen, and Guankui Long*

Cite This: *Nano Lett.* 2026, 26, 3090−3097 Read Online

ACCESS | Metrics & More | Article Recommendations | Supporting Information

ABSTRACT: Chiral hybrid organic−inorganic metal halides (HOIMHs) with noncentrosymmetric structure have attracted significant attention for nonlinear optics (NLO). Herein, guided by atom response theory (ART), we screened representative lead-free metal halide polyhedra and found that $[NbCl_6]^-$ exhibits the highest linear polarizability. Therefore, we constructed the first chiral niobium-based HOIMHs, (*R*/*S*-3BrMBA)$NbCl_6$ (***R*/*S*-Nb**), and investigated their NLO properties. As expected, ***S*-Nb** exhibits efficient second harmonic generation (SHG) under 770−1000 nm excitation. Most importantly, the effective second-order NLO coefficient (d_{eff}) of ***S*-Nb** reaches 6.77 pm/V, representing the highest value among the reported zero-dimensional chiral HOIMHs. Moreover, ***S*-Nb** demonstrates strong SHG circular dichroism (SHG-CD) under circularly polarized excitation, with an anisotropy factor ($g_{SHG\text{-}CD}$) of 1.37, which is one of the highest values among chiral HOIMHs. Our results highlight the potential of chiral niobium halides toward nonlinear chiroptical applications and provide an effective ART-guided strategy for designing high-performance NLO material through polarizability and band-gap engineering.

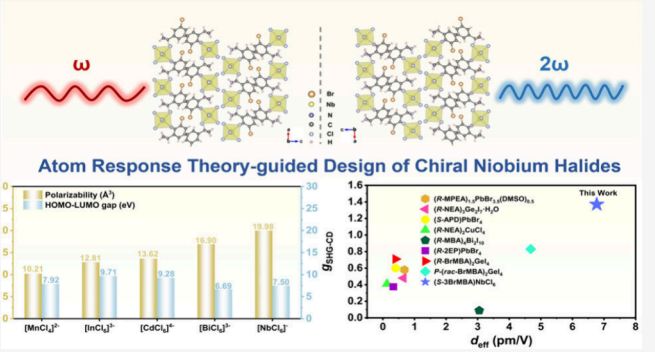

KEYWORDS: *chiral niobium halide, atom response theory, polarizability, nonlinear optics, second harmonic generation*

Nonlinear optics (NLO) plays a vital role in contemporary photonics and optoelectronics,[1,2] such as frequency conversion,[3,4] optical switching,[5,6] and quantum information processing.[7,8] Specifically, second harmonic generation (SHG), the most fundamental and significant second-order NLO process,[9−11] directly generates frequency-doubled coherent radiation through a two-photon combination process, which is critically important in fields such as laser technology, precise metrology, and bioimaging.[12−15] The discovery and design of SHG materials with a strong NLO response is a primary goal for achieving highly efficient NLO devices.[16]

Recent research based on atom response theory (ART) has established a semiquantitative linear relationship for the nonlinear coefficient (d_{eff}), as shown in eq 1[17,18]

$$d_{eff} \propto \frac{\alpha_{sum}}{NE_g} \quad (1)$$

where α_{sum} denotes the total cell polarizability, N represents the atom count per unit cell, and E_g represents the band gap. Therefore, designing a NLO material that simultaneously owns high α_{sum} and narrow band gaps at a comparable N could achieve a higher d_{eff}. Within this principle, diverse structural units with high polarizability,[19−21] such as pentaborates,[18,22] π-conjugated fragments,[23] chalcogenides,[24] and second-order Jahn−Teller distorted transition octahedra were introduced to construct the NLO materials.[25] To implement this strategy, chiral hybrid organic−inorganic metal halides (HOIMHs) are ideal platforms, due to their structural diversity and compositional tunability.[26,27] Most importantly, chiral HOIMHs inherently crystallize into noncentrosymmetric (NCS) space groups,[28,29] making them highly promising for both linear[30−37] and nonlinear chiroptical applications.[38−48] However, most of the reported chiral HOIMHs still rely on lead, which poses serious environmental concerns. Thus, developing lead-free chiral HOIMHs based on novel metal centers is highly needed. On the other hand, considering that α_{sum} fundamentally depends on the polarizability of the constituent structural units,[49,50]

Received: November 26, 2025
Revised: February 20, 2026
Accepted: February 23, 2026
Published: February 27, 2026

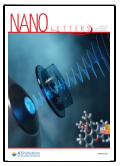

https://doi.org/10.1021/acs.nanolett.5c05945
Nano Lett. 2026, 26, 3090−3097

screening the lead-free polyhedral units with high intrinsic linear polarizability (α) is highly needed.

Using density functional theory (DFT),[51] we calculated the linear polarizability and HOMO−LUMO gap of representative lead-free metal chloride polyhedra, including $[MnCl_4]^{2-}$, $[InCl_6]^{3-}$, $[CdCl_6]^{4-}$, $[BiCl_6]^{3-}$, and $[NbCl_6]^{-}$. $[NbCl_6]^{-}$ exhibits the highest linear polarizability, together with a narrow HOMO−LUMO gap, among these units (Figure 1). Accordingly, the $\alpha_{sum}/(NE_g)$ of $[NbCl_6]^{-}$ significantly surpasses that of the other metal halide polyhedra (Figure S1), and the chiral HOIMHs based on the $[NbCl_6]^{-}$ unit should exhibit superior nonlinear-optical properties. On the one hand, considering that lithium niobate ($LiNbO_3$, LBO) is one of the most widely used NLO materials in both nonlinear wavelength conversion and electro-optic modulation,[52−54] we first developed the niobium-based chiral HOIMHs, (*R*/*S*-3BrMBA)$NbCl_6$ (***R*/*S*-Nb**), with a systematic investigation of their NLO properties in this work. Single-crystal structure analysis and circular dichroism (CD) confirm the successful chirality transfer from the chiral cations to the inorganic niobium (V) halide framework. The valence band maximum (VBM) originates primarily from the chiral cations, whereas the conduction band minimum (CBM) exists predominantly on niobium (V) chloride. As expected, ***S*-Nb** exhibits efficient SHG under 770−1000 nm excitation, with a SHG intensity at 500 nm that is 128 times stronger than Y-cut quartz. More importantly, ***S*-Nb** achieves d_{eff} of 6.77 pm/V, representing the highest value for reported zero-dimensional (0D) chiral HOIMHs. On the other hand, an efficient SHG-CD under circularly polarized excitation (LCP and RCP) is also observed, with an anisotropy factor (g_{SHG-CD}) of 1.37, making it one of the highest values yet reported for chiral HOIMHs. Therefore, chiral niobium (V) chlorides exhibit both a high nonlinear coefficient and a large anisotropy factor and are promising candidates toward nonlinear chiroptical applications. Our work presents an effective ART-guided strategy for increasing the nonlinear coefficient of chiral HOIMHs through rational polarizability and band-gap engineering, which offers valuable insights into designing highly efficient NLO materials toward real applications.

The chiral niobium-based HOIMHs ***R*/*S*-Nb** were synthesized through the cooling-induced crystallization of $NbCl_5$ and 1-(3-bromophenyl)ethylammonium (3-BrMBACl) in thionyl chloride (Figure S2). ***R*/*S*-Nb** crystals crystallize into the orthorhombic space group of $P2_12_12_1$ with nearly identical unit cell parameters, confirming their enantiomerism (Figure S3 and Table S1). As shown in Figure 2a, the isolated $[NbCl_6]^{-}$ octahedra in ***R*/*S*-Nb** are surrounded by chiral cations (*R*/*S*-3BrMBA$^+$) and connected through Coulombic force and N−H···Cl hydrogen bonding (Figures 2b and S5). To further analyze these hydrogen-bonding interactions, Hirshfeld surface analyses and corresponding two-dimensional (2D) fingerprint plots were performed (Figures S6 and S7). The results show that N−H···Cl interactions account for approximately 48% of the total interactions and confirm the dominant role of stabilizing the crystal structure. These hydrogen bonds formed between chiral organic cations and inorganic $[NbCl_6]^{-}$ octahedra directly induce distortions in the inorganic octahedra. The Cl−Nb−Cl bond angle in ***R*/*S*-Nb** deviates significantly from 180° to approximately 177°, while the Nb−Cl bond length ranges from 2.300 to 2.381 Å (Figure S5). The bond length distortion index (D) and bond angle variance (σ^2) are adopted to quantitatively assess these octahedral distortions, as described in eqs 2 and 3[55]

$$D = \frac{1}{6}\sum_{i=1}^{6}\frac{|d_i - d_0|}{d_0} \tag{2}$$

$$\sigma^2 = \frac{1}{11}\sum_{i=1}^{12}(\theta_i - 90)^2 \tag{3}$$

where d_i is a specific Nb−Cl bond length, d_0 signifies the averaged Nb−Cl bond length, and θ_i denotes the Cl−Nb−Cl bond angle. The calculated D for both ***R*-Nb** and ***S*-Nb** is *ca.* 0.0109, which is much larger than that of $[MnCl_4]^{2-}$, $[InCl_6]^{3-}$, $[CdCl_6]^{4-}$, and $[BiCl_6]^{3-}$.[38−41] This larger D for ***R*-Nb** and ***S*-Nb** should originate from the asymmetric N−H···Cl hydrogen-bonding network inducted by the chiral organic cations, which could also promote the innate second-order Jahn−Teller distortion of the Nb^{5+} ($4d^0$) center. The calculated σ^2 values are 3.5492 and 3.4936 for ***R*-Nb** and ***S*-Nb**, respectively, results that are larger than those of $[MnCl_4]^{2-}$ and $[InCl_6]^{3-}$. These large structural distortions could increase the polarizability anisotropy of ***R*/*S*-Nb**, thus contributing to the stronger NLO response, as discussed below.

The powder X-ray diffraction (PXRD) patterns of ***R*/*S*-Nb** show excellent correspondence with the simulated patterns,

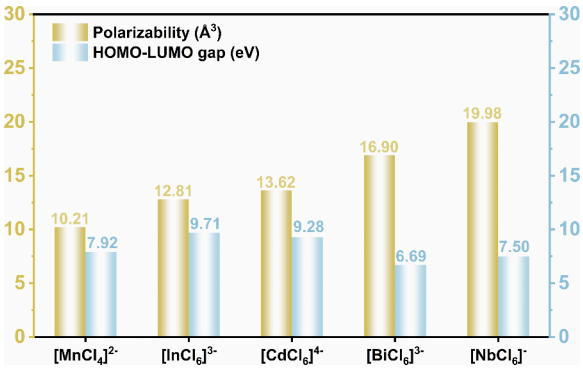

Figure 1. Calculated linear polarizability and HOMO−LUMO gap of representative lead-free metal chloride polyhedra based on DFT (ωB97X-D/6-31G*).

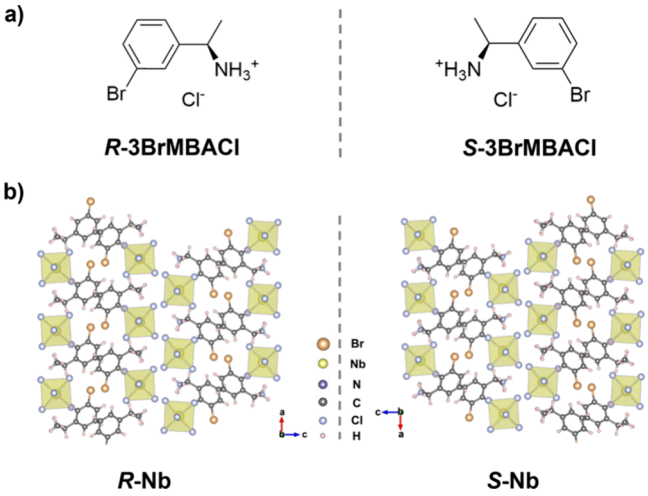

Figure 2. Crystal structure of ***R*/*S*-Nb**. (a) Chemical structures of chiral organic cations: (*R*)- and (*S*)-3BrMBACl. (b) Crystal structures viewed along the *b* axis.

https://doi.org/10.1021/acs.nanolett.5c05945
Nano Lett. 2026, 26, 3090−3097

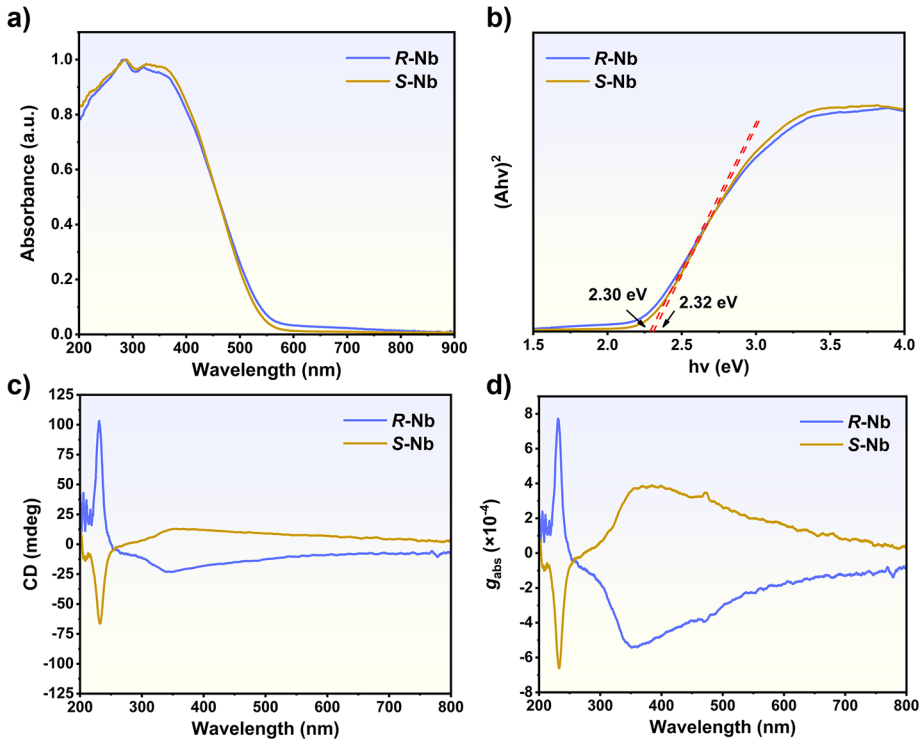

Figure 3. (a) UV−vis DRS of ***R*/*S*-Nb**. (b) Tauc plot of ***R*/*S*-Nb**. (c) CD spectra of ***R*/*S*-Nb**. (d) Corresponding g_{abs} spectra of ***R*/*S*-Nb**.

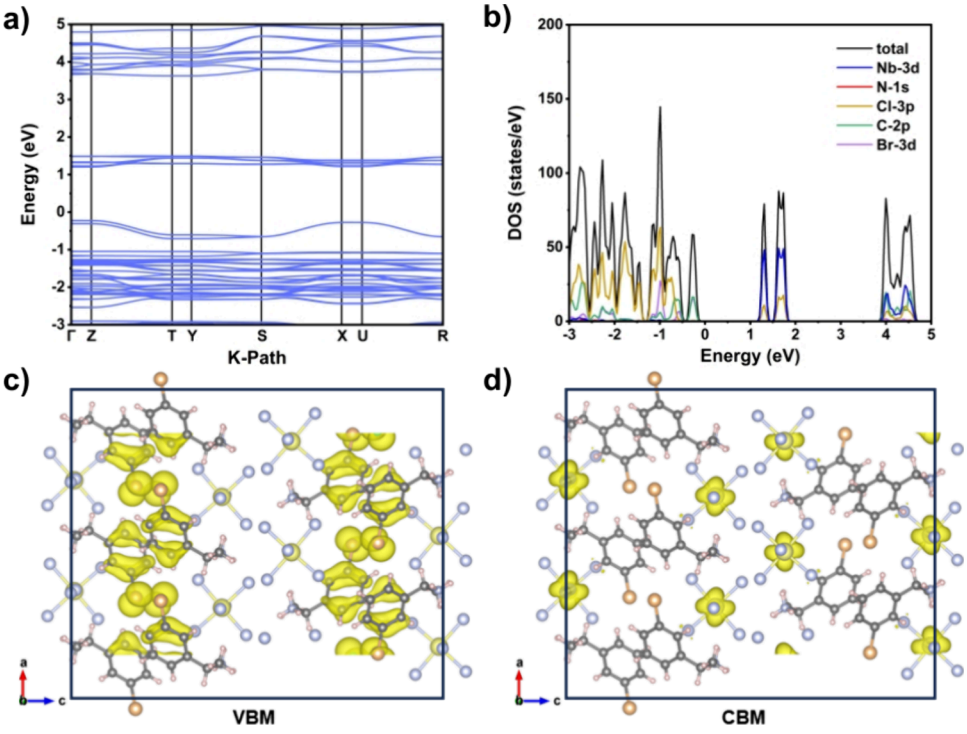

Figure 4. (a) Calculated electronic band structures of ***S*-Nb**. (b) Calculated PDOS of ***S*-Nb**. (c and d) Charge density maps associated with the VBM and CBM of ***S*-Nb**.

revealing high phase purity (Figure S8). X-ray photoelectron spectroscopy (XPS) also verifies the existence of N, C, Nb, and Cl (Figures S9 and S10). The XPS peaks at around 207.0 and 209.4 eV correspond to Nb $3d_{5/2}$ and Nb $3d_{3/2}$, respectively, further confirming the existence of Nb^{5+} in *R*- and *S*-Nb.[56] The Fourier transform infrared (FTIR) spectra of ***R*/*S*-Nb** exhibit characteristic peaks at 1218 and 1574 cm^{-1}, assignable to the C−N stretching and N−H bending modes of *R*/*S*-3BrMBA, respectively (Figure S11).

The UV−vis diffuse-reflectance spectroscopy (DRS) spectra were performed to investigate the linear optical response of ***R*/*S*-Nb**. Both enantiomers exhibit nearly identical strong absorption in the UV region (Figure 3a). The optical band gap of ***R*/*S*-Nb** was estimated to be *ca.* 2.3 eV from Tauc plot analysis (Figure

https://doi.org/10.1021/acs.nanolett.5c05945
Nano Lett. 2026, 26, 3090−3097

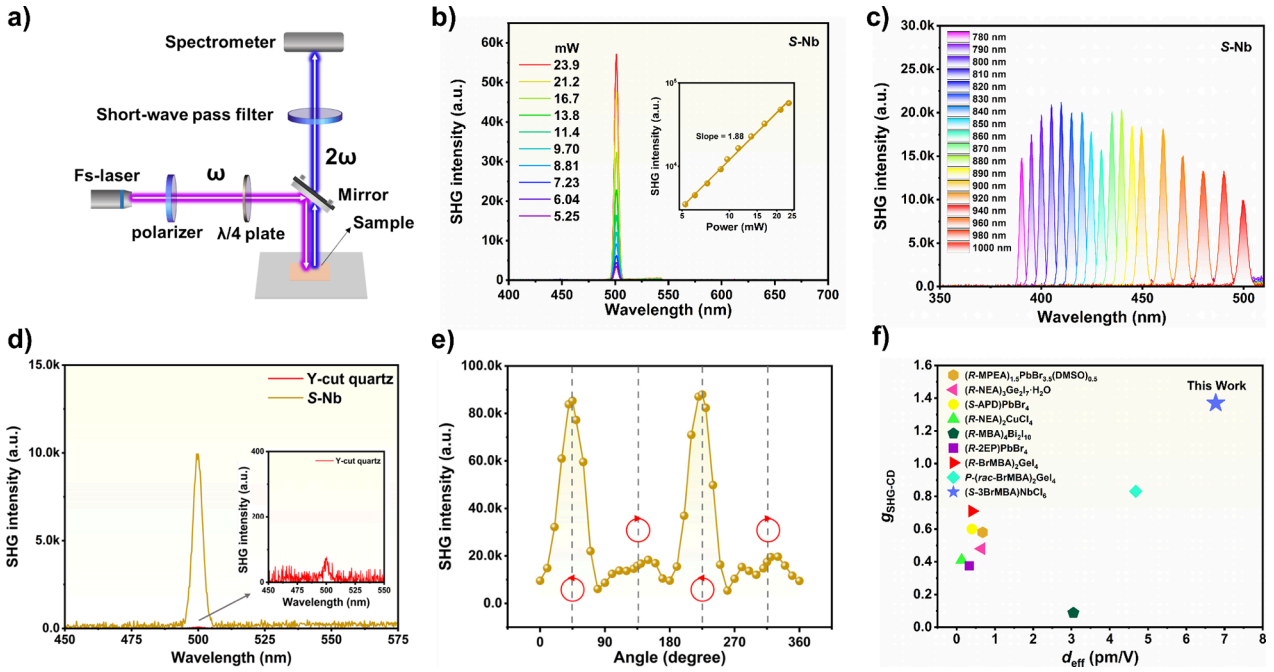

Figure 5. (a) Schematic diagram of the microarea NLO measurements. (b) Excitation-power-dependent SHG spectra of the ***S*-Nb** film at 500 nm, with the corresponding log−log dependence of the SHG intensity versus pump power. (c) Wavelength-dependent SHG response of ***S*-Nb**. (d) Relative SHG intensity of ***S*-Nb** compared with quartz under identical conditions. (e) Polarization-resolved SHG intensity of ***S*-Nb** versus $\lambda/4$ plate angle (λ = 1000 nm). (f) Comparative analysis of $g_{SHG\text{-}CD}$ and d_{eff} values between this work and previously reported systems.

3b). Furthermore, ***R*-Nb** and ***S*-Nb** exhibit mirror-image CD signals with the Cotton effect, with the 350 nm peak originating from ligand-to-metal charge transfer within the $[NbCl_6]^-$ octahedra (Figure 3c),[57] which are distinct from the chiral-cation-dominated CD peak at 240 nm (Figure S12). Therefore, chirality transfer from the chiral organic cations to the inorganic frameworks is achieved. The anisotropy factor (g_{abs}) of ***R*-Nb** at 350 nm is calculated to be *ca.* 4×10^{-4} (Figure 3d) using the formula $g_{abs} = \theta\ (mdeg)/(32980 \cdot Abs)$,[58] comparable to values reported for chiral HOIMHs.

We performed DFT calculations to probe the electronic band structure and partial density of states (PDOS) of ***R*/*S*-Nb**.[59] The resulting band structure reveals a direct band gap in the Brillouin zone (Figure S13), with both the VBM and CBM situated at the Γ point (Figure 4a). The VBM originates primarily from C 2p and N 2p orbitals of the chiral organic cations, while the CBM is governed mainly by the Nb 3d and Cl 3p states (Figures 4b and S14b). Therefore, the wave functions further confirm obvious charge transfer from the chiral organic cations (VBM) to the $[NbCl_6]^-$ octahedra (CBM) (Figures 4c,d and S14).[60,61] Furthermore, the UV−vis absorption spectra and corresponding Tauc plots reveal a distinct band-gap narrowing in ***R*/*S*-Nb** compared to $NbCl_5$ and *R*/*S*-3BrMBACl (Figure S15). Our DFT calculations indicate that the band gap of the inorganic part in ***R*/*S*-Nb** remains nearly unchanged compared to that of the $NbCl_5$ precursor (*ca.* 2.2 eV, Figure S16). Therefore, the observed band-gap narrowing should be attributed to organic−inorganic charge transfer. We further performed a transition dipole moment calculation, which also confirmed the weak charge-transferred nature (Figure S17).

The NCS structure of ***R*/*S*-Nb** endows them with pronounced second-order NLO properties. To facilitate the SHG measurements, the ***R*/*S*-Nb** films were prepared (refer to the experimental details in the Supporting Information). As confirmed by PXRD, the prominent diffraction peaks of the films closely correspond to those of the powders, confirming that the films maintain the crystal structure of ***R*/*S*-Nb** (Figure S18). According to the energy-dispersive X-ray spectroscopy (EDS) elemental maps, C, N, Nb, and Cl exhibit a spatially uniform distribution within the ***R*/*S*-Nb** films, indicating good compositional homogeneity (Figures S19 and S20). Then the SHG measurements were performed on the ***R*/*S*-Nb** films by using a reflective microarea NLO measurements system with vertical excitation (Figure 5a). The excitation source was a femtosecond pulsed laser (140 fs, 80 MHz), and the beam was focused on the samples through a microscope objective. The SHG intensity exhibits a quadratic relationship with the incident laser power, with fitted slopes of 1.88 for ***S*-Nb** (Figure 5b) and 1.86 for ***R*-Nb** (Figure S22b), respectively, confirming the second-order nature of the NLO response. A clear frequency-doubling peak was consistently observed at 500 nm under 1000 nm excitation. The wavelength-dependent SHG measurements revealed distinct responses across 770−1000 nm, with SHG signals appearing at exactly half of the fundamental wavelength, demonstrating a robust and broadband second-order NLO response extending well into the infrared region (Figure 5c). Quantitative analysis was performed using Y-cut quartz as the standard under identical excitation conditions (Figure S21), revealing that the SHG intensity of ***S*-Nb** is enhanced by approximately 128 times compared with quartz at 500 nm (Figure 5d). Moreover, the SHG measurements were also conducted on the ***R*-Nb** films, which exhibit nearly identical behavior with that of ***S*-Nb** (Figure S22). Furthermore, to quantitatively assess the NLO performance, the d_{eff} of ***R*/*S*-Nb** was calculated based on eq 4[62]

$$\frac{d^s_{eff}}{d^y_{eff}} \approx \sqrt{\frac{I^s_{2\omega}}{I^y_{2\omega}}}\frac{I^y_{\omega}}{I^s_{\omega}}\frac{n^s_{\omega}}{n^y_{\omega}}\sqrt{\frac{n^s_{2\omega}}{n^y_{2\omega}}} \tag{4}$$

where d^s_{eff} and d^y_{eff} represent the effective second-order nonlinear coefficients of the ***R*/*S*-Nb** films and Y-cut quartz, respectively.

https://doi.org/10.1021/acs.nanolett.5c05945
Nano Lett. 2026, 26, 3090−3097

The d_{eff} value of Y-cut quartz is *ca.* 0.6 pm/V.[63] I_ω signifies the fundamental pump intensity, $I_{2\omega}$ indicates the output SHG intensity, and n_ω and $n_{2\omega}$ correspond to the refractive indices at the fundamental frequencies ω and second-harmonic frequencies 2ω, respectively. The refractive index of the ***R*/*S*-Nb** film is 1.56 at 1000 nm and 1.61 at 500 nm based on our measurements, while it is 1.48 (1000 nm) and 1.55 (500 nm) for Y-cut quartz, respectively. Based on the quantitative analysis, d_{eff} of ***S*-Nb** reaches 6.77 pm/V, outperforming all previously reported 0D HOIMHs (Figure S24 and Table S2).

The intrinsic enantiomeric nature of ***R*-** and ***S*-Nb** also endows them with both CD and SHG capabilities, thus resulting in the polarization-dependent SHG response. To evaluate the SHG-CD response, the SHG measurements of the samples were carried out under LCP and RCP produced by a quarter-wave plate. Significant SHG intensity differences are observed for ***R*-** and ***S*-Nb** (Figures 5e and S23). The SHG-CD effect was quantified by rotating a $\lambda/4$ plate to generate circularly polarized excitation, and the anisotropy factor ($g_{SHG\text{-}CD}$) was subsequently determined according to eq 5

$$g_{SHG\text{-}CD} = 2\frac{I^{L}_{SHG\text{-}CD} - I^{R}_{SHG}}{I^{L}_{SHG} + I^{R}_{SHG}} \quad (5)$$

where I^{L}_{SHG} and I^{R}_{SHG} correspond to the SHG intensities excited by LCP and RCP lasers, respectively. The obtained anisotropy factor is 1.37 for ***S*-Nb**, representing one of the highest values among the reported chiral HOIMHs (Figure S25 and Table S3). Therefore, chiral niobium(V) halides exhibit not only a high d_{eff} but also a strong chirality-driven NLO response (Figure 5f), which are promising toward nonlinear chiroptical applications.

In summary, the first chiral niobium-based HOIMHs, (*R*/*S*-3BrMBA)$NbCl_6$ (***R*/*S*-Nb**), were successfully constructed based on screening the linear polarizability of the representative lead-free metal halide polyhedra under the guidance of ART. Single-crystal structures and CD provide evidence for the successful chirality transfer from the chiral organic cations to the inorganic niobium (V) halides. As expected, ***S*-Nb** exhibits a strong second-order NLO response under 770−1000 nm excitation, with an SHG intensity 128 times that of quartz at 500 nm. A d_{eff} of 6.77 pm/V is achieved for ***S*-Nb**, surpassing all other reported values for 0D chiral HOIMHs. More importantly, ***S*-Nb** also possesses strong SHG-CD with $g_{SHG\text{-}CD}$ as high as 1.37, representing one of the highest values among the reported chiral HOIMHs. These findings not only confirm the effectiveness of an ART-guided NLO material design principle through polarizability and band-gap engineering but also highlight the significant potential of chiral niobium (V) chlorides toward advanced nonlinear chiroptical applications.

■ ASSOCIATED CONTENT

Data Availability Statement

CCDC 2488417 and 2488418 contain the supplementary crystallographic data for this paper. These data can be obtained free of charge via www.ccdc.cam.ac.uk/data_request/cif, or by emailing data_request@ccdc.cam.ac.uk, or by contacting The Cambridge Crystallographic Data Centre, 12 Union Road, Cambridge CB2 1EZ, UK; fax: + 44 1223 336033.

Supporting Information

The Supporting Information is available free of charge at https://pubs.acs.org/doi/10.1021/acs.nanolett.5c05945.

Material synthesis details, calculation methods, crystal structure data, calculated (α_{sum}/NE_g) value, crystal photographs, SEM images, EDS mapping, XRD patterns, FTIR spectra, XPS spectra, CD and absorption spectra, and supplementary SHG data (PDF)

■ AUTHOR INFORMATION

Corresponding Author

Guankui Long − *Frontiers Science Center for New Organic Matter, Tianjin Key Laboratory for Rare Earth Materials and Applications, Renewable Energy Conversion and Storage Center (RECAST), School of Materials Science and Engineering, National Institute for Advanced Materials, Nankai University, Tianjin 300350, China;* orcid.org/0000-0002-1826-3736; Email: longgk09@nankai.edu.cn

Authors

Wenting Liu − *Frontiers Science Center for New Organic Matter, Tianjin Key Laboratory for Rare Earth Materials and Applications, Renewable Energy Conversion and Storage Center (RECAST), School of Materials Science and Engineering, National Institute for Advanced Materials, Nankai University, Tianjin 300350, China*

Xin Zeng − *Frontiers Science Center for New Organic Matter, Tianjin Key Laboratory for Rare Earth Materials and Applications, Renewable Energy Conversion and Storage Center (RECAST), School of Materials Science and Engineering, National Institute for Advanced Materials, Nankai University, Tianjin 300350, China*

Wenkai Zhao − *Frontiers Science Center for New Organic Matter, Tianjin Key Laboratory for Rare Earth Materials and Applications, Renewable Energy Conversion and Storage Center (RECAST), School of Materials Science and Engineering, National Institute for Advanced Materials, Nankai University, Tianjin 300350, China*

Haolin Lu − *Frontiers Science Center for New Organic Matter, Tianjin Key Laboratory for Rare Earth Materials and Applications, Renewable Energy Conversion and Storage Center (RECAST), School of Materials Science and Engineering, National Institute for Advanced Materials, Nankai University, Tianjin 300350, China*

Hebin Wang − *Frontiers Science Center for New Organic Matter, Tianjin Key Laboratory for Rare Earth Materials and Applications, Renewable Energy Conversion and Storage Center (RECAST), School of Materials Science and Engineering, National Institute for Advanced Materials, Nankai University, Tianjin 300350, China*

Xinyi Niu − *Frontiers Science Center for New Organic Matter, Tianjin Key Laboratory for Rare Earth Materials and Applications, Renewable Energy Conversion and Storage Center (RECAST), School of Materials Science and Engineering, National Institute for Advanced Materials, Nankai University, Tianjin 300350, China*

Zhaoyu Wang − *Frontiers Science Center for New Organic Matter, Tianjin Key Laboratory for Rare Earth Materials and Applications, Renewable Energy Conversion and Storage Center (RECAST), School of Materials Science and Engineering, National Institute for Advanced Materials, Nankai University, Tianjin 300350, China;* orcid.org/0009-0007-3785-7218

Tianyin Shao − *Frontiers Science Center for New Organic Matter, Tianjin Key Laboratory for Rare Earth Materials and*

https://doi.org/10.1021/acs.nanolett.5c05945
Nano Lett. 2026, 26, 3090−3097

Applications, Renewable Energy Conversion and Storage Center (RECAST), School of Materials Science and Engineering, National Institute for Advanced Materials, Nankai University, Tianjin 300350, China

Sehrish Gull − *Frontiers Science Center for New Organic Matter, Tianjin Key Laboratory for Rare Earth Materials and Applications, Renewable Energy Conversion and Storage Center (RECAST), School of Materials Science and Engineering, National Institute for Advanced Materials, Nankai University, Tianjin 300350, China*

Bing Sun − *State Key Laboratory of Natural Product Chemistry (SKLAOC), Key Laboratory of Special Function Materials and Structure Design (MOE), College of Chemistry and Chemical Engineering, Lanzhou University, Lanzhou 730000, China*

Hao-Li Zhang − *State Key Laboratory of Natural Product Chemistry (SKLAOC), Key Laboratory of Special Function Materials and Structure Design (MOE), College of Chemistry and Chemical Engineering, Lanzhou University, Lanzhou 730000, China;* orcid.org/0000-0002-6322-5202

Xinfeng Liu − *CAS Key Laboratory of Standardization and Measurement for Nanotechnology, National Center for Nanoscience and Technology, Beijing 100190, China;* orcid.org/0000-0002-7662-7171

Yongsheng Chen − *The Centre of Nanoscale Science and Technology and Key Laboratory of Functional Polymer Materials, Institute of Polymer Chemistry, Renewable Energy Conversion and Storage Center (RECAST), College of Chemistry, Nankai University, Tianjin 300071, China;* orcid.org/0000-0003-1448-8177

Complete contact information is available at: https://pubs.acs.org/10.1021/acs.nanolett.5c05945

Author Contributions

†W.L. and X.Z. contributed equally to this work.

Notes

The authors declare no competing financial interest.

■ ACKNOWLEDGMENTS

The authors gratefully acknowledge financial support from the National Natural Science Foundation of China (52473305, 92256202, 52541104, U22A20399, and 22405111), the Fundamental Research Funds for the Central Universities, Nankai University (Grant 023-63233038), and the 111 Project (B18030). All theoretical calculations were performed at the Supercomputing Center of Lanzhou University.

■ REFERENCES

(1) Braidotti, M. C.; Faccio, D.; Wright, E. M. Penrose Superradiance in Nonlinear Optics. *Phys. Rev. Lett.* **2020**, *125* (19), No. 193902.

(2) Dutt, A.; Mohanty, A.; Gaeta, A. L.; Lipson, M. Nonlinear and Quantum Photonics Using Integrated Optical Materials. *Nat. Rev. Mater.* **2024**, *9* (5), 321−346.

(3) Wang, Z.-Y.; Wu, X.; Xiong, X.; Yang, C.; Hao, Z.; Yang, Q.-F.; Hu, Y.; Bo, F.; Cao, Q.-T.; Xiao, Y.-F. Toward Ultimate-Efficiency Frequency Conversion in Nonlinear Optical Microresonators. *Sci. Adv.* **2025**, *11* (18), No. eadu7605.

(4) Pang, Z.; Arie, A. Coherence Synthesis in Nonlinear Optics. *Light: Sci. Appl.* **2025**, *14*, 101.

(5) Pshenichnyuk, I. A.; Yousry, F.; Zemtsov, D. S.; Kosolobov, S. S.; Drachev, V. P. Nonlinear Optical Switching in Hybrid Plasmonic Waveguides. *Phys. Rev. B* **2024**, *109* (3), No. 35401.

(6) Biswal, B. P.; Valligatla, S.; Wang, M.; Banerjee, T.; Saad, N. A.; Mariserla, B. M. K.; Chandrasekhar, N.; Becker, D.; Addicoat, M.; Senkovska, I.; Berger, R.; Rao, D. N.; Kaskel, S.; Feng, X. Nonlinear Optical Switching in Regioregular Porphyrin Covalent Organic Frameworks. *Angew. Chem., Int. Ed.* **2019**, *58* (21), 6896−6900.

(7) Cui, C.; Seshadreesan, K. P.; Guha, S.; Fan, L. High-Dimensional Frequency-Encoded Quantum Information Processing with Passive Photonics and Time-Resolving Detection. *Phys. Rev. Lett.* **2020**, *124* (19), No. 190502.

(8) Tiarks, D.; Schmidt-Eberle, S.; Stolz, T.; Rempe, G.; Dürr, S. A Photon−Photon Quantum Gate Based on Rydberg Interactions. *Nat. Phys.* **2019**, *15* (2), 124−126.

(9) He, W.; Chen, C.; Wu, S.; Wong, W. P. D.; Wu, Z.; Chang, K.; Wang, J.; Gao, H.; Loh, K. P. Dion−Jacobson Perovskites with a Ferroelectrically Switchable Chiral Nonlinear Optical Response. *J. Am. Chem. Soc.* **2025**, *147* (1), 811−820.

(10) Okada, D.; Araoka, F. Electric-Field-Induced Giant Resonant Enhancement of Second Harmonic Generation in Two-Dimensional Hybrid Perovskite. *J. Am. Chem. Soc.* **2025**, *147* (17), 14677−14683.

(11) Goulielmakis, E.; Brabec, T. High Harmonic Generation in Condensed Matter. *Nat. Photonics* **2022**, *16* (6), 411−421.

(12) Yuan, Z.; Ge, J.; Liu, P.; Li, B.; Li, M.; Liu, J.-Y.; Yu, Y.; Chen, H.-J.; Bowers, J.; Vahala, K. Efficient and Wavelength-Tunable Second-Harmonic Generation toward the Green Gap. *Sci. Adv.* **2025**, *11* (27), No. eadw2781.

(13) Li, X.; Bian, Y.; Xia, C.; Zhao, B.; Ma, S.; Wang, J.; Qiu, H.; Liu, H.; Liu, M.; Yu, H.; Ye, N.; Hu, Z.; Wu, Y. Enhanced Second-Harmonic Generation in Quadratically Nonlinear Weyl Semimetal NbAs for Broadband Photodetection Applications. *Adv. Funct. Mater.* **2025**, *35* (14), No. 2418485.

(14) Qi, X.; Liu, H.; Guo, W.; Lin, W.; Lin, B.; Jin, Y.; Deng, X. New Opportunities: Second Harmonic Generation of Boron-Doped Graphene Quantum Dots for Stem Cells Imaging and Ultraprecise Tracking in Wound Healing. *Adv. Funct. Mater.* **2019**, *29* (37), No. 1902235.

(15) Lee, S.; Poojari, C. S.; Maznichenko, A.; Roesel, D.; Swiderska, I.; Pohl, P.; Hub, J. S.; Roke, S. Dynamic Second Harmonic Imaging of Proton Translocation Through Water Needles in Lipid Membranes. *J. Am. Chem. Soc.* **2024**, *146* (29), 19818−19827.

(16) Kuzyk, M. G.; Perez-Moreno, J.; Shafei, S. Sum Rules and Scaling in Nonlinear Optics. *Phys. Rep.* **2013**, *529* (4), 297−398.

(17) Ding, B.; Cheng, X.; Mi, H.; Köhler, J.; Yang, Q.; Yang, T.; Deng, S. Insight into the Origin of Second Harmonic Generation and Rational Design in the Metal Halide Borates. *Inorg. Chem.* **2025**, *64* (2), 1153−1163.

(18) Cheng, X.; Li, Z.; Wu, X.-T.; Hong, M.; Whangbo, M.-H.; Deng, S. Key Factors Controlling the Large Second Harmonic Generation in Nonlinear Optical Materials. *ACS Appl. Mater. Interfaces* **2020**, *12* (8), 9434−9439.

(19) Ward, J.; Miller, C. Measurements of Nonlinear Optical Polarizabilities for Twelve Small Molecules. *Phys. Rev. A* **1979**, *19* (2), 826.

(20) Li, G.; Zhang, S.; Zentgraf, T. Nonlinear Photonic Metasurfaces. *Nat. Rev. Mater.* **2017**, *2* (5), 1−14.

(21) Wu, C.; Jiang, X.; Hu, Y.; Jiang, C.; Wu, T.; Lin, Z.; Huang, Z.; Humphrey, M. G.; Zhang, C. A Lanthanum Ammonium Sulfate Double Salt with a Strong SHG Response and Wide Deep-UV Transparency. *Angew. Chem., Int. Ed.* **2022**, *61* (6), No. e202115855.

(22) Cheng, X.; Whangbo, M.-H.; Hong, M.; Deng, S. Dependence of the Second-Harmonic Generation Response on the Cell Volume to Band-Gap Ratio. *Inorg. Chem.* **2019**, *58* (15), 9572−9575.

(23) Wu, L.; Lin, C.; Tian, H.; Zhou, Y.; Fan, H.; Yang, S.; Ye, N.; Luo, M. Mg $(C_3O_4H_2)(H_2O)_2$: A New Ultraviolet Nonlinear Optical Material Derived from $KBe_2BO_3F_2$ with High Performance and Excellent Water-Resistance. *Angew. Chem., Int. Ed.* **2024**, *63* (2), No. e202315647.

(24) Chen, M.-C.; Wu, L.-M.; Lin, H.; Zhou, L.-J.; Chen, L. Disconnection Enhances the Second Harmonic Generation Response:

Synthesis and Characterization of $Ba_{23}Ga_8Sb_2S_{38}$. *J. Am. Chem. Soc.* **2012**, *134* (14), 6058−6060.
(25) Hu, Y.; Wu, C.; Jiang, X.; Duanmu, K.; Huang, Z.; Lin, Z.; Humphrey, M. G.; Zhang, C. Ultrashort Phase-Matching Wavelength and Strong Second-Harmonic Generation in Deep-UV-Transparent Oxyfluorides by Covalency Reduction. *Angew. Chem., Int. Ed.* **2023**, *62* (52), No. e202315133.
(26) Ma, W.; Liang, D.; Qian, Q.; Mo, Q.; Zhao, S.; Cai, W.; Chen, J.; Zang, Z. Near-Unity Quantum Yield in Zero-Dimensional Lead-Free Manganese-Based Halides for Flexible X-Ray Imaging with High Spatial Resolution. *eScience* **2023**, *3* (2), No. 100089.
(27) Zhu, C.; Jin, J.; Wang, Z.; Xu, Z.; Folgueras, M. C.; Jiang, Y.; Uzundal, C. B.; Le, H. K. D.; Wang, F.; Zheng, X.; Yang, P. Supramolecular Assembly of Blue and Green Halide Perovskites with Near-Unity Photoluminescence. *Science* **2024**, *383* (6678), 86−93.
(28) Pietropaolo, A.; Mattoni, A.; Pica, G.; Fortino, M.; Schifino, G.; Grancini, G. Rationalizing the Design and Implementation of Chiral Hybrid Perovskites. *Chem.* **2022**, *8* (5), 1231−1253.
(29) Kim, H.; Choi, W.; Kim, Y. J.; Kim, J.; Ahn, J.; Song, I.; Kwak, M.; Kim, J.; Park, J.; Yoo, D.; Park, J.; Kwak, S. K.; Oh, J. H. Giant Chiral Amplification of Chiral 2D Perovskites Via Dynamic Crystal Reconstruction. *Sci. Adv.* **2024**, *10* (34), No. eado5942.
(30) Niu, X.; Li, Y.; Lu, H.; Wang, Z.; Zhang, Y.; Shao, T.; Wang, H.; Gull, S.; Sun, B.; Zhang, H.; Chen, Y.; Wang, K.; Du, Y.; Long, G. Chiral Europium Halides with High-Performance Magnetic Field Tunable Red Circularly Polarized Luminescence at Room Temperature. *Nat. Commun.* **2025**, *16*, 2525.
(31) Shi, C.-M.; Lu, H.; Wang, J.-Y.; Long, G.; Xu, L.-J.; Chen, Z.-N. Stepwise Amplification of Circularly Polarized Luminescence in Indium-Based Metal Halides by Regulating Their Structural Dimension. *Nat. Commun.* **2025**, *16*, 1505.
(32) Long, G.; Sabatini, R.; Saidaminov, M. I.; Lakhwani, G.; Rasmita, A.; Liu, X.; Sargent, E. H.; Gao, W. Chiral-Perovskite Optoelectronics. *Nat. Rev. Mater.* **2020**, *5* (6), 423−439.
(33) Long, G.; Jiang, C.; Sabatini, R.; Yang, Z.; Wei, M.; Quan, L. N.; Liang, Q.; Rasmita, A.; Askerka, M.; Walters, G.; Gong, X.; Xing, J.; Wen, X.; Quintero-Bermudez, R.; Yuan, H.; Xing, G.; Wang, X. R.; Song, D.; Voznyy, O.; Zhang, M.; Hoogland, S.; Gao, W.; Xiong, Q.; Sargent, E. H. Spin Control in Reduced-Dimensional Chiral Perovskites. *Nat. Photonics* **2018**, *12* (9), 528−533.
(34) Ye, C.; Jiang, J.; Zou, S.; Mi, W.; Xiao, Y. Core−Shell Three-Dimensional Perovskite Nanocrystals with Chiral-Induced Spin Selectivity for Room-Temperature Spin Light-Emitting Diodes. *J. Am. Chem. Soc.* **2022**, *144* (22), 9707−9714.
(35) Liu, Y.; Luo, Z.; Wei, Y.; Li, C.; Chen, Y.; He, X.; Chang, X.; Quan, Z. Integrating Achiral and Chiral Organic Ligands in Zero-Dimensional Hybrid Metal Halides to Boost Circularly Polarized Luminescence. *Angew. Chem., Int. Ed.* **2023**, *62* (37), No. e202306821.
(36) Chen, Q.; Ding, Z.; Zhang, L.; Wang, D.; Geng, C.; Feng, Y.; Zhang, J.; Ren, M.; Li, S.; Qaid, S. M.; Jiang, Y.; Yuan, M. Uniaxial-Oriented Chiral Perovskite for Flexible Full-Stokes Polarimeter. *Adv. Mater.* **2024**, *36* (29), No. 2400493.
(37) Liu, S.; Zerhoch, J.; Heindl, M. W.; Zhang, C.; Kodalle, T.; Sun, K.; Shcherbakov, A.; Bodnar, S.; Miah, M.; Gholipoor, M.; Jandl, C.; Pöthig, A.; Ballmann, J.; Sharp, I. D.; Müller-Buschbaum, P.; Sutter-Fella, C. M.; Paetzold, U. W.; Deschler, F. Orientation-Driven Chirality Funnels in Chiral Low-Dimensional Lead-Halide Perovskite Heterostructures. *J. Am. Chem. Soc.* **2025**, *147* (19), 16681−16693.
(38) Zheng, X.; Liu, Y.; Liu, G.; Liu, J.; Ye, X.; Han, Q.; Ge, C.; Tao, X. Crystalline Mixed Halide Halobismuthates and Their Induced Second Harmonic Generation. *Chem. Mater.* **2016**, *28* (12), 4421−4431.
(39) Ye, H.; Hu, W.-H.; Chen, X.-X.; Zhao, B.-Q.; Zhang, W.-X.; Chen, X.-M. Heat- and Pressure-Driven Room-Temperature Polymorphic Transition Accompanied with Switchable SHG Signal in a New Chiral Hexagonal Perovskite. *Chem. Asian J.* **2023**, *18* (19), No. e202300608.
(40) Chen, P.; Jiao, S.; Tang, Z.; Sun, X.; Li, D.; Yang, Z.; Lu, Y.; Zhang, W.; Cai, H.-L.; Wu, X. A Room Temperature Ferroelectric Material with Photoluminescence: $(1,3\text{-Dicyclohexylimidazole})_2MnCl_4$. *Dalton Trans.* **2023**, *52* (27), 9448−9455.
(41) Deng, Y.; Li, F.; Zhou, Z.; Wang, M.; Zhu, Y.; Zhao, J.; Liu, S.; Zhao, Q. Chiral Induction and Sb^{3+} Doping in Indium Halides to Trigger Second Harmonic Generation and Circularly Polarized Luminescence. *Chin. Chem. Lett.* **2024**, *35* (8), No. 109085.
(42) Guo, Z.; Li, J.; Liang, J.; Wang, C.; Zhu, X.; He, T. Regulating Optical Activity and Anisotropic Second-Harmonic Generation in Zero-Dimensional Hybrid Copper Halides. *Nano Lett.* **2022**, *22* (2), 846−852.
(43) Wu, J.; Chang, T.; Yang, Z.; Zan, H.; Bai, Y.; Han, X.; Luo, N.; Yuan, M.; Zeng, R. Magneto-Chiroptical Hybrid Perovskites with Anomalous Photovoltaic Effect for High-Performance Self-Driven Photodetectors. *Adv. Mater.* **2025**, *37* (38), No. 2509074.
(44) Song, X. J.; Qin, Y.; Ai, Y.; Chen, X. G.; Weng, Y. R.; Peng, H.; Lv, H. P.; Xiong, R. G.; Liao, W. Q. Mathematical Double-Matrix Switchable Homochiral Ferroelectric. *Angew. Chem., Int. Ed.* **2025**, *64* (36), No. e202507554.
(45) Wang, H.; Li, J. J.; Lu, H.; Gull, S.; Shao, T.; Zhang, Y.; He, T.; Chen, Y.; He, T.; Long, G. Chiral Hybrid Germanium (II) Halide with Strong Nonlinear Chiroptical Properties. *Angew. Chem., Int. Ed.* **2023**, *62* (41), No. e202309600.
(46) Yu, J.; Li, M.; Lv, Y.; Liao, B.; Tan, G.; Zou, J.; Liu, X.; Han, Y.; Li, L. Second-Harmonic-Generation Circular-Dichroism in Chiral Perovskite Single Crystals Enhanced by Self-Trapped Excitonic State. *Adv. Funct. Mater.* **2026**, *36*, No. e08904.
(47) Yuan, C.; Li, X.; Semin, S.; Feng, Y.; Rasing, T.; Xu, J. Chiral Lead Halide Perovskite Nanowires for Second-Order Nonlinear Optics. *Nano Lett.* **2018**, *18* (9), 5411−5417.
(48) Maniadi, M.; Mercier, N.; Abhervé, A.; Gindre, D.; Tailleur, E.; Pillet, S.; Dupray, V.; Tyrpenou, C.; Volonakis, G. A 2D Double Perovskite Based on the Chiral Cystaminium Cation Exhibiting Multiple Switches in Quadratic Nonlinear Optical Response. *J. Am. Chem. Soc.* **2025**, *147* (44), 40708−40718.
(49) Long, Y.; Dong, X.; Huang, L.; Zeng, H.; Lin, Z.; Zhou, L.; Zou, G. $BaSb(H_2PO_2)_3Cl_2$: An Excellent UV Nonlinear Optical Hypophosphite Exhibiting Strong Second-Harmonic Generation Response. *Mater. Today Phys.* **2022**, *28*, No. 100876.
(50) Wu, L.; Lin, C.; Tian, H.; Yan, T.; Li, B. X.; Fan, H.; Fan, Y.; Yang, S.; Luo, M. Engineering an Excellent B-BaB_2O_4-Inspired UV Nonlinear Optical Material through Secondary Building Unit Substitution. *Angew. Chem., Int. Ed.* **2025**, *64* (22), No. e202500877.
(51) Bhandari, S.; Cheung, M. S.; Geva, E.; Kronik, L.; Dunietz, B. D. Fundamental Gaps of Condensed-Phase Organic Semiconductors from Single-Molecule Calculations using Polarization-Consistent Optimally Tuned Screened Range-Separated Hybrid Functionals. *J. Chem. Theory Comput.* **2018**, *14* (12), 6287−6294.
(52) Dutto, F.; Raillon, C.; Schenk, K.; Radenovic, A. Nonlinear Optical Response in Single Alkaline Niobate Nanowires. *Nano Lett.* **2011**, *11* (6), 2517−2521.
(53) Talts, Ü. L.; Weigand, H.; Occhiodori, I.; Grange, R. Scalable Lithium Niobate Nanoimprinting for Nonlinear Metalenses. *Adv. Mater.* **2025**, *37* (27), No. 2418957.
(54) Chen, P.-K.; Briggs, I.; Cui, C.; Zhang, L.; Shah, M.; Fan, L. Adapted Poling to Break the Nonlinear Efficiency Limit in Nanophotonic Lithium Niobate Waveguides. *Nat. Nanotechnol.* **2024**, *19* (1), 44−50.
(55) Robinson, K.; Gibbs, G.; Ribbe, P. Quadratic Elongation: A Quantitative Measure of Distortion in Coordination Polyhedra. *Science* **1971**, *172* (3983), 567−570.
(56) Atuchin, V.; Kalabin, I.; Kesler, V.; Pervukhina, N. Nb 3d and O 1s Core Levels and Chemical Bonding in Niobates. *J. Electron Spectrosc. Relat. Phenom.* **2005**, *142* (2), 129−134.
(57) Brisdon, B.; Fowles, G.; Tidmarsh, D.; Walton, R. Complex Halides of Transition Metals—VIII: A Comparative Study of the Electronic Absorption Spectra of the ZrX_6^{2-} HfX_6^{2-}-NbX_6^- and TaX_6^- Anions. *Spectrochim. Acta, Part A* **1969**, *25* (5), 999−1007.
(58) Gong, Z.; Zhu, X.; Zhou, Z.; Zhang, S.; Yang, D.; Zhao, B.; Zhang, Y.; Deng, J.; Cheng, Y.; Zheng, Y.; Zang, S.; Kuang, H.; Duan,

https://doi.org/10.1021/acs.nanolett.5c05945
Nano Lett. 2026, 26, 3090−3097

P.; Yuan, M.; Chen, C.; Zhao, Y.; Zhong, Y.; Tang, B.; Liu, M. Frontiers in Circularly Polarized Luminescence: Molecular Design, Self-Assembly, Nanomaterials, and Applications. *Sci. China Chem.* **2021**, *64* (12), 2060−2104.
(59) Kresse, G.; Furthmüller, J. Efficient Iterative Schemes for Ab Initio Total-Energy Calculations Using a Plane-Wave Basis Set. *Phys. Rev. B* **1996**, *54* (16), No. 11169.
(60) Jia, Q.; Zhang, Z.; Ni, H.; Lin, Q.; Teri, G.; Liu, P.; Luo, J.; Huang, P.; Wang, Z.; Wang, C.; Liu, Z.; Zhang, Y.; Fu, D.-W. Polarization-Switching Controlled Luminescence in Hybrid Ferroelectric. *Angew. Chem., Int. Ed.* **2025**, *64* (42), No. e202505163.
(61) Yan, S.-F.; Guo, Y.; Liu, W.; Guo, S.-P.; Wu, J. Tellurium (IV) Halide Achieving Effective Nonlinear-Optical Activity: The Role of Chiral Ligands and Lattice Distortion. *Inorg. Chem.* **2024**, *63* (1), 73−77.
(62) Theodossiou, T. A.; Thrasivoulou, C.; Ekwobi, C.; Becker, D. L. Second Harmonic Generation Confocal Microscopy of Collagen Type I from Rat Tendon Cryosections. *Biophys. J.* **2006**, *91* (12), 4665−4677.
(63) Guo, Z.; Li, J.; Wang, C.; Liu, R.; Liang, J.; Gao, Y.; Cheng, J.; Zhang, W.; Zhu, X.; Pan, R.; He, T. Giant Optical Activity and Second Harmonic Generation in 2D Hybrid Copper Halides. *Angew. Chem., Int. Ed.* **2021**, *60* (15), 8441−8445.

https://doi.org/10.1021/acs.nanolett.5c05945
Nano Lett. 2026, 26, 3090−3097